Journal of Power Sources 271 (2014) 213–222

Contents lists available at ScienceDirect

Journal of Power Sources

journal homepage: www.elsevier.com/locate/jpowsour

Long-term behaviour of solid oxide fuel cell interconnect materials in contact with Ni-mesh during exposure in simulated anode gas at 700 and 800 °C

L. Garcia-Fresnillo, V. Shemet, A. Chyrkin*, L.G.J. de Haart, W.J. Quadakkers

Forschungszentrum Jülich, Institute of Energy and Climate Research, 52425 Jülich, Germany

HIGHLIGHTS

- Material behaviour in a real SOFC stack is reported (exposure up to 3000 h).
- Interdiffusion between high Cr ferritic steel and Ni-mesh results in precipitation of σ-phase in the reaction zone.
- The mechanism of σ-phase precipitation is discussed in terms of alloy thermodynamics (CALPHAD approach).
- Effect of alloying elements, e.g. W and Nb, on the σ-phase stability is clarified.

ARTICLE INFO

Article history:
Received 21 May 2014
Received in revised form
14 July 2014
Accepted 31 July 2014
Available online 7 August 2014

Keywords:
Interconnect
Ni-mesh
Interdiffusion
Ferritic steel
σ-phase

ABSTRACT

In the present study the long-term behaviour of two ferritic steels, Crofer 22 APU and Crofer 22H, in contact with a Ni-mesh during exposure in simulated anode gas, Ar–4%H_2–2%H_2O, at 700 and 800 °C for exposure times up to 3000 h was investigated. Ni diffusion from the Ni-mesh into the steel resulted in the formation of an austenitic zone whereas diffusion of iron and chromium from the steel into the Ni-mesh resulted in the formation of chromia base oxides in the Ni-mesh. Depending on the chemical composition of the steel, the temperature and the exposure time, interdiffusion processes between ferritic steel and Ni-mesh also resulted in σ-phase formation at the austenite–ferrite interface and in Laves-phase dissolution in the austenitic zone. The extent and morphology of the σ-phase formation are discussed on the basis of thermodynamic considerations, including reaction paths in the ternary alloy system Fe–Ni–Cr.

1. Introduction

Interconnect plates are used in planar solid oxide fuel cells (SOFC's) to separate the different atmospheres present at the cathode and the anode side, thus serving as current collector as well as electrical connectors. Chromia-forming alloys, such as ferritic steels or Cr-base ODS alloys, have been successfully used as interconnect materials since chromia has a reasonably good electronic conductivity at the high service temperatures [1–6]. The overall electrical resistance of the interconnect material is directly related to the thickness of the chromia layer, which means that after long-term exposure at high temperatures, the electrical resistance values might reach unacceptably high levels for the proper operation of the cell [7–10]. The overall performance of the cell can be enhanced by improving the electrical contact between the anode and the interconnector using an intermediate Ni-mesh between the anode and the interconnector. Nonetheless, the long-term interaction between the Ni-mesh and the interconnector material, involving interdiffusion of different alloying elements, may adversely affect the long-term performance of the cell.

The major concern of using a Ni-mesh in direct contact with a ferritic steel interconnect is that the presence of nickel results in the formation of an austenitic γ-FCC phase in the ferritic steel in the contact zone [11–18]. This phase transformation is associated with a volume change and a change in the physical and mechanical properties of the interconnect material in the contact zone. Austenite possesses a substantially higher coefficient of thermal expansion than ferrite, which may result in initiation of mechanical stresses during thermal cycling [19–22]. Additionally, the interdiffusion coefficients of chromium and nickel are approximately 30 times lower in austenite than in the ferrite [23,24]. The slower chromium diffusion in the austenite may adversely affect the

* Corresponding author. Tel.: +49 2461 61 5537; fax: +49 2461 61 3699.
E-mail address: a.chyrkin@fz-juelich.de (A. Chyrkin).

http://dx.doi.org/10.1016/j.jpowsour.2014.07.189
0378-7753/

selective oxidation of Cr in the interconnect steel and thus, the formation and growth of a protective chromia base surface scale [19–21,25]. The width of the austenitic zone is expected to increase with exposure time since Cr depletion as result of chromia scale growth implies that less Fe and Ni are needed to stabilize the γ-FCC phase.

Apart from austenite formation, interdiffusion between the interconnect material and the Ni-mesh are known to lead to phase transformations and microstructural changes in the interconnect material. Formation of σ-phase near the contact area between a Ni-mesh and the ferritic steel Crofer 22H has been observed after exposure in Ar–4%H_2–2%H_2O at 800 °C for 1000 h [18]. Niewolak et al. [12] found that σ-FeCr precipitates formed in the interdiffusion zone, i.e. at the interface between the original ferritic matrix and the austenite, when Crofer 22 APU electroplated with a 5–10 μm thick Ni layer was exposed in Ar–9.2%CO–3.7H_2–0.2% H_2O at 600 °C for 300 h. Presence of the brittle σ-phase may be a source for crack formation and therefore decrease the overall performance of the interconnect.

Also the properties of the Ni-mesh may be affected by interdiffusion processes. Nickel oxide is thermodynamically not stable at the equilibrium oxygen partial pressure prevailing in the anode gas. Nonetheless, Fe, Cr, and other alloying elements from the interconnector material may diffuse into the Ni-mesh driven by elemental activity gradients, and different types of oxides with low electrical conductivity might form on the Ni surface and thus reduce the cathode area [26].

The present study investigates the long-term behaviour of two commercial ferritic steels in contact with a Ni-mesh during exposure in simulated anode gas, Ar–4%H_2–2%H_2O, in the temperature range 700–800 °C for exposure times up to 3000 h. After exposure the specimens were characterized using light optical metallography scanning electron microscopy (SEM), energy and wavelength dispersive X-ray spectroscopy (EDX/WDX) and electron backscatter diffraction (EBSD). In the investigations main emphasis was put on the interdiffusion of alloying elements between the Ni-mesh and the interconnect materials, on surface oxide formation as well as on phase formation and dissolution in the interdiffusion zone.

2. Experimental

The long-term behaviour of a Ni-mesh in contact with two high chromium ferritic steels was studied using the commercial materials Crofer 22 APU and Crofer 22H [27–29]. The detailed alloy chemical composition, analyzed by inductively coupled plasma-optical emission spectroscopy (ICP-OES) and infrared (IR) analysis, is listed in Table 1. The contact between the Ni-mesh and the interconnect steels was accomplished by spot-welding.

The samples were exposed in simulated anode gas, Ar–4% H_2–2%H_2O, for exposure times of 1000 and 3000 h at 700 and 800 °C. The equilibrium oxygen partial pressures in this gas are 1.1×10^{-19} bar at 800 °C and 3.6×10^{-22} bar at 700 °C. The exposures were carried out in a horizontal furnace, whereby the specimens were placed in a longitudinal crucible. A sintered alumina crucible was used in order to avoid specimen contamination by the formation of volatile silicon containing species which form in gases with low oxygen potential when silica glass or silica containing ceramics are used as specimen holders [30].

The oxidized specimens were embedded in an epoxy resin and subsequently cross-sections were prepared for metallographic analyses using conventional techniques, i.e. grinding, polishing and fine polishing. The metallographic cross-sections were characterized by optical metallography and scanning electron microscopy (SEM) with energy and wavelength dispersive X-ray spectroscopy (EDX/WDX) as well as electron backscatter diffraction (EBSD).

3. Results

3.1. Crofer 22 APU

The long-term exposure of the nickel/Crofer 22 APU joints in simulated anode gas at 700 and 800 °C leads to interdiffusion of alloy elements between the Ni-mesh and the steel. Interdiffusion profiles showed that Ni diffuses from the Ni-mesh into the steel resulting in the formation of austenite grains in the contact zone between the Ni-mesh and the steel (Fig. 1). The Ni diffusion distance into the steel has been measured from the interdiffusion profiles between the Ni-mesh and the steel. Fig. 2 shows that the Ni penetration increases with increasing time and increasing temperature. The austenitic zone does not only increase in direction perpendicular to the original steel surface but it also spreads longitudinally. It was observed that the shape of the austenitic zone was more uneven after exposure at 800 °C than after exposure at 700 °C.

After exposure at 700 °C minor amounts of an intermetallic phase were found at the interface between the original ferritic matrix and the austenitic zone (Fig. 3). EDX analyses indicated that these precipitates contain 57.7 at.% Fe, 39.3 at.% Cr, 2.4 at.% Ni and 0.6 at.% Mn, a chemical composition which corresponds to σ-phase [31]. After 3000 exposure hours σ-phase precipitates could be observed not only at the austenite–ferrite interface but also within the austenitic zone. No indication of σ-phase formation was observed after exposure at 800 °C.

The diffusion of Fe, Cr and Mn from the steel into the Ni-mesh results in oxide formation in the Ni-mesh. According to SEM analysis a thin Cr-rich oxide layer with an outer Cr-/Mn-spinel formed on the surface of the Ni-mesh whereas some Cr-, Mn-oxides, which followed an irregular pattern, formed inside the Ni-mesh (Fig. 4).

On the surface of Crofer 22 APU which was not in contact with the Ni-mesh, a Cr-rich oxide layer formed under all studied conditions. SEM analysis revealed that it mainly consisted of Cr_2O_3 with an outer Cr-/Mn-spinel. Some whiskers could be observed in the outer surface of the oxide scale (Fig. 5a), in agreement with previous observations showing that Cr-/Mn-spinel tends to exhibit whisker type morphology in water vapour rich, low pO_2 gases [30,32]. Additionally, some pores were present near the interface between outer spinel and inner chromia layer, which is also in agreement with previous observations.

In addition to the investigated model samples, an SOFC stack which used Crofer 22 APU as interconnect material in contact with a Ni-mesh was investigated after 18000 service hours at 800 °C. Metallographic cross-sections and BSE images revealed that

Table 1
Chemical composition in weight % of studied batches of ferritic steels Crofer 22 APU and Crofer 22H analyzed by inductively coupled plasma-optical emission spectroscopy (ICP-OES) and infrared (IR) analysis.

	Fe	Cr	Mn	Si	Nb	W	Al	Ti	La	C	N
Crofer 22 APU	Base	23.0	0.42	<0.01	<0.01	<0.01	<0.01	0.058	0.052	<0.001	0.003
Crofer 22H	Base	22.7	0.42	0.31	0.56	1.98	<0.01	0.060	0.064	0.0025	0.0233

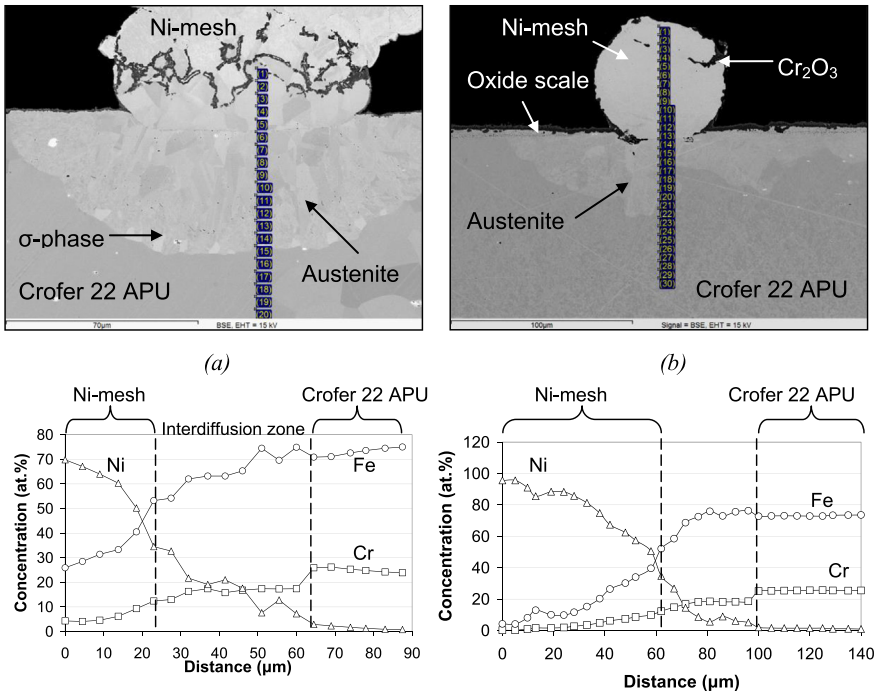

Fig. 1. BSE images of Crofer 22 APU in contact with Ni-mesh after exposure in simulated anode gas, Ar–4%H_2–2%H_2O, for 1000 h; (a) at 700 °C and (b) at 800 °C. Lower part of the figure shows interdiffusion profiles between the Ni-mesh and Crofer 22 APU along lines indicated in upper figures.

diffusion of Ni into the steel and of Cr, Fe into the Ni-mesh resulted in partial austenitization of the interconnect and in the formation of oxides in the Ni-mesh (Fig. 6). The findings were qualitatively in accordance with the results of the model experiments. It was found that a chromia layer formed on the surface of the Ni-mesh and some internal oxidation along Ni-mesh grain boundaries was observed, although the oxide morphology differs from those observed in the previous studies. No indication of σ-phase formation in the ferritic steel was found (Fig. 6).

3.2. Crofer 22H

Diffusion of different alloying elements between the Ni-mesh and the ferritic steel Crofer 22H occurred when the material was exposed at 700 °C and at 800 °C in simulated anode gas, Ar–4% H_2–2%H_2O, for exposure times up to 3000 h.

As in the case of Crofer 22 APU, nickel diffusion from the nickel-mesh into the steel resulted in the formation of an austenitic zone in the contact area (Fig. 7). The Ni diffusion distance into the steel measured from the interdiffusion profiles between the Ni-mesh and the steel (Fig. 2) indicates that the Ni diffusion distance initially increases with increasing time. However, after approximately 2000 h nickel does not diffuse much deeper into the ferritic steel but tends to reach an asymptotic value. The measured Ni diffusion depths after exposure at 800 °C are only slightly higher than the values measured after exposure at 700 °C.

Precipitates of σ-phase were found to be formed at the interface between the ferritic steel and the austenitic zone after 1000 h exposure at 700 °C as well as at 800 °C. EDX analysis revealed an approximate chemical composition for the σ-phase of 58.4 at.% Fe, 37.1 at.% Cr, 2 at.% Ni, 1.7 at.% W and 0.8 at.% Mn. The amount of σ-phase formed at 700 °C was larger than that formed at 800 °C. After 1000 exposure hours at 700 °C, approximately 47 vol. % of σ-phase was estimated to form in the austenitic zone whereas only sporadic precipitates were found after the same exposure time at 800 °C. After 3000 h exposure no clear indication of σ-phase formation was observed at 800 °C whereas after the same exposure time at 700 °C numerous elongated σ-phase precipitates could be found (Fig. 8).

The diffusion of Cr, Fe and Mn from the steel into the Ni-mesh resulted in the oxidation of the Ni-mesh. BSE images showed that, apart from a Cr-rich layer with an outer Cr-/Mn-spinel which formed on the surface of the Ni-mesh, some oxides formed inside the Ni-mesh. This internal oxidation was especially noticeable after exposure at 700 °C for 3000 h and it seems to take place at a certain distance from the contact point between the Ni-mesh and the steel. Element mappings from EDX analyses showed that these oxides are Cr-rich although they also contained Mn and minor amounts of W and Nb (Fig. 9).

A Cr-rich oxide layer formed on Crofer 22H during exposure in Ar–4%H_2–2%H_2O in areas which were not in contact with the Ni-

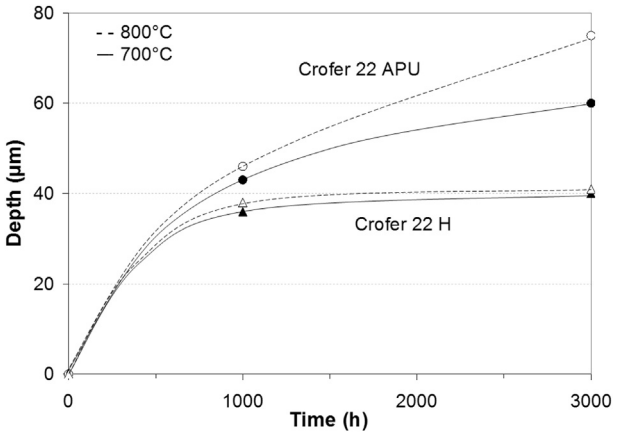

Fig. 2. Maximum Ni diffusion depth into the steel as function of exposure time in simulated anode gas, Ar–4%H_2–2%H_2O, at 700 and 800 °C. The lines were inserted for clearer visibility of the results.

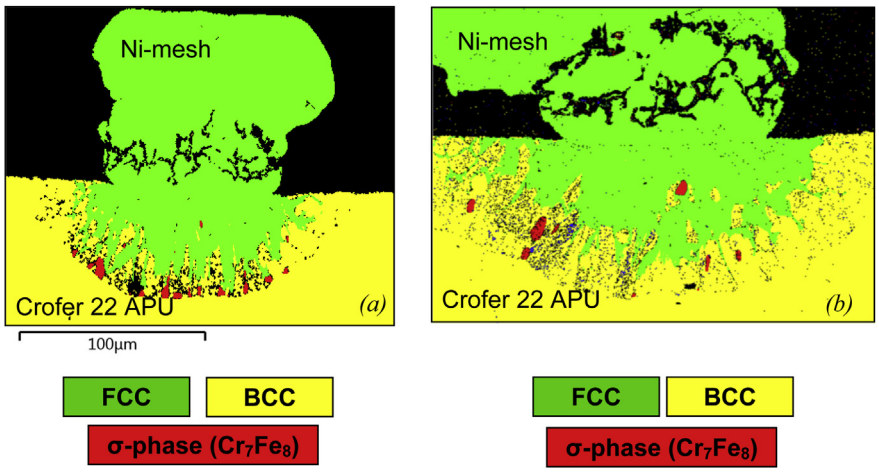

Fig. 3. EBSD phase maps of Crofer 22 APU in contact with Ni-mesh after exposure in simulated anode gas, Ar–4%H_2–2%H_2O, at 700 °C for; (a) 1000 h and (b) 3000 h.

mesh. EDX analyses revealed that the oxide scale consists of a Cr_2O_3 layer with an outer Cr-/Mn-spinel. As already observed for Crofer 22 APU, (Fig. 5a) the Cr-/Mn-spinel exhibited whisker type morphology and some pores formed near the chromia–spinel interface in agreement with previous observations (Fig. 5b).

The creep strength of Crofer 22H is mainly governed by solid-solution strengthening and precipitation of strengthening by Fe_2(W,Nb) Laves-phase [22,33]. Laves-phase was present in the microstructure of Crofer 22H both at the grain boundaries as well as within the alloy grains (Figs. 7 and 9). However, Laves-phase seems

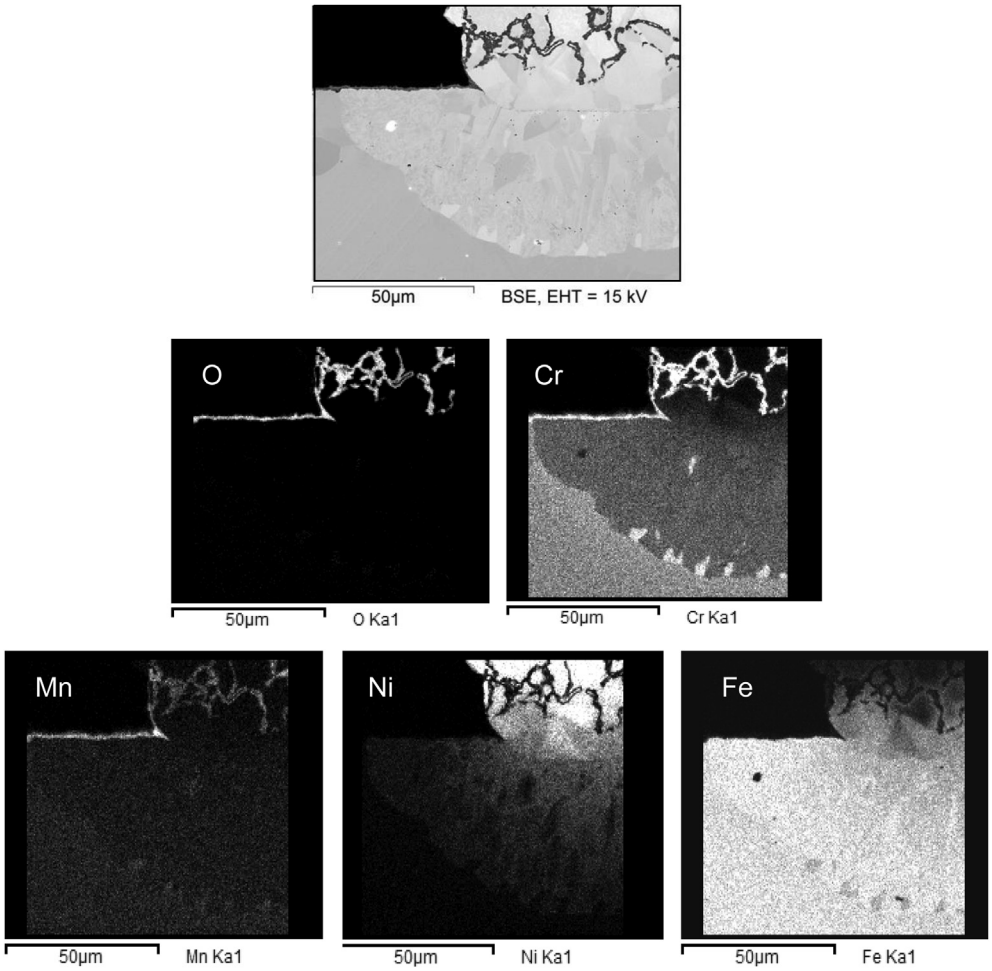

Fig. 4. BSE images of Crofer 22 APU in contact with Ni-mesh after exposure in simulated anode gas, Ar–4%H_2–2%H_2O, at 700 °C for 1000 h. Lower part of the figure shows X-ray mappings of the elements Cr, O, Fe, Mn, Ni.

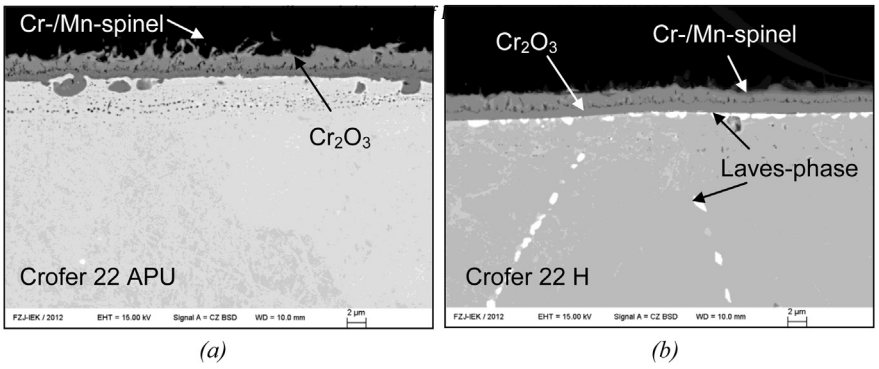

Fig. 5. BSE images of (a) Crofer 22 APU and (b) Crofer 22H after exposure in simulated anode gas, Ar−4%H_2−2%H_2O, for 1000 h at 800 °C.

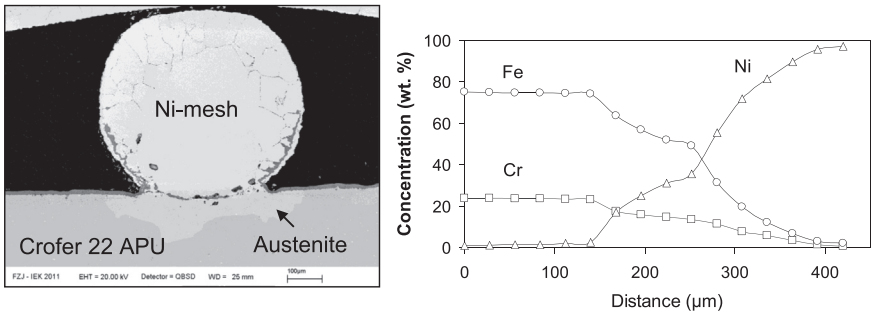

Fig. 6. BSE image and concentration profiles of Fe, Ni and Cr across contact zone between Crofer 22 APU in a real SOFC stack and Ni-mesh after 18000 service hours at 800 °C.

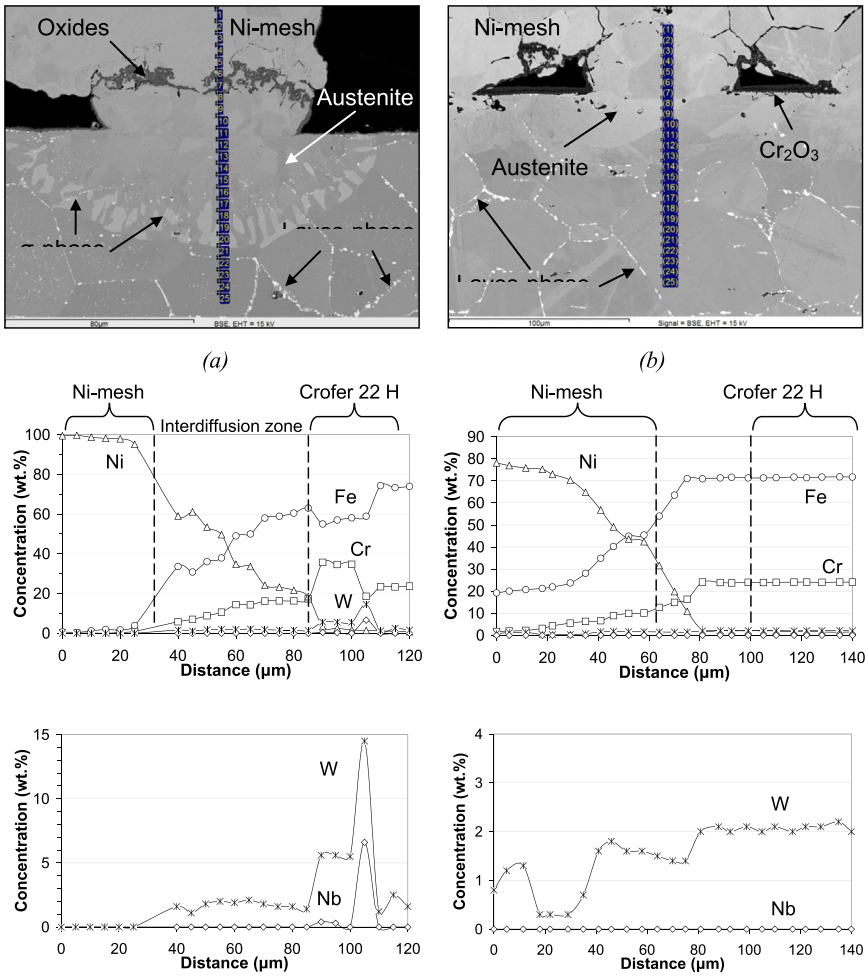

Fig. 7. BSE images of Crofer 22H in contact with a Ni-mesh after exposure in simulated anode gas, Ar−4%H_2−2%H_2O, for 3000 h; (a) at 700 °C and (b) at 800 °C. Lower figures show interdiffusion profiles between the Ni-mesh and Crofer 22H along lines indicated in upper figures.

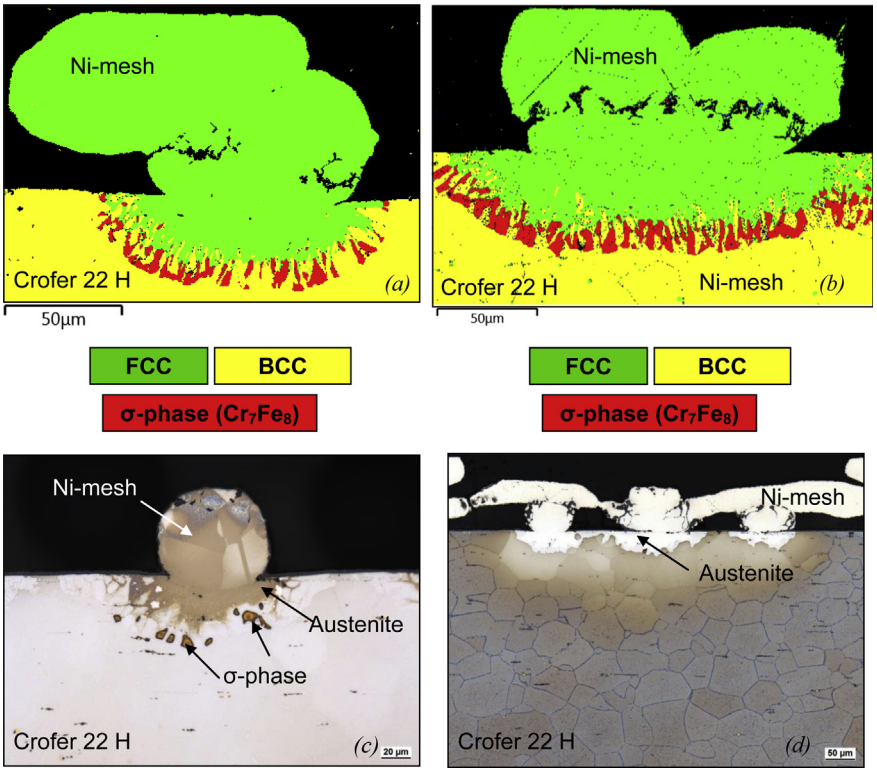

Fig. 8. (a)(b) EBSD phase maps of Crofer 22H in contact with a Ni-mesh after exposure in simulated anode gas, Ar–4%H_2–2%H_2O at 700 °C for (a) 1000 h and (b) 3000 h; (c)(d) light optical microscopy images showing metallographic cross-sections of Crofer 22H in contact with Ni-mesh after exposure in simulated anode gas, Ar–4%H_2–2%H_2O, at 800 °C for (a) 1000 h and (b) 3000 h (Electrochemical etching in 10% NaOH at 1.5 V for 7 s).

hardly be present in the austenitic zone; only few, small particles of Laves-phase were found within this zone.

In those parts of the steel which were not in contact with the Ni-mesh, an enrichment of Laves-phase in the immediate vicinity of the Cr-rich oxide layer followed by a zone in which Laves-phase was depleted, was observed. Enrichment-depletion of Laves-phase in the subsurface zone of Crofer 22H has been previously reported by Asensio et al. and was attributed to Nb uphill diffusion in the subscale Cr-depletion profile as well as to preferential nucleation at the scale–alloy interface [29,34,35].

4. Discussion

Interdiffusion processes between the Ni-mesh and the ferritic steels Crofer 22 APU and Crofer 22H during exposure in simulated anode gas leads to the formation of an austenitic zone in the steel. Apart from this phenomenon formation of an intermetallic phase, i.e. σ-phase, at the interface between the ferritic steel and the austenitic zone has been observed. The formation of this phase depends on time, temperature and steel composition.

In the case of Crofer 22 APU the σ-phase was found after exposure at 700 °C for 1000 and 3000 h but it was not observed after exposure at 800 °C. In Crofer 22H the σ-phase was present after 1000 h exposure at 700 as well as 800 °C. However, σ-phase precipitates were no longer present when the material was exposed at 800 °C for 3000 h.

For obtaining a more detailed insight at the σ-phase formation in case of Crofer 22 APU after exposure at 700 °C for 1000 and 3000 h the experimentally measured points of the interdiffusion profiles between the Ni-mesh and steel were inserted into the Ni–Fe–Cr ternary phase diagram at 700 °C and the diffusion path of the system was traced (Fig. 10). In the interdiffusion profiles it can be observed that the chromium content in the steel at the ferrite–austenite interface increases up to a value of 26 approximately wt.% (Fig 1). This experimentally observed local Cr-enrichment can be explained if a diffusion couple between pure nickel and a ferritic steel is considered (Fig. 11). In the diffusion couple at the nickel–ferrite interface there are three diffusion processes occurring at the same time; Fe and Cr diffuse from the steel into the Ni-mesh whereas Ni diffuses from the Ni-mesh into the steel (Fig. 11). The flux j_i of the element i, is defined according to Fick's first law as:

$$j_i = -D_i \frac{dC_i}{dx}$$

where D_i is the diffusion coefficient of the element i, and dC_i/dx is the concentration gradient. The interdiffusion coefficient of iron and chromium in nickel at 700 °C are $\tilde{D}^{Ni}_{FeFe} = 5.0 \times 10^{-20}$ m^2 s^{-1} and $\tilde{D}^{Ni}_{CrCr} = 4.9 \times 10^{-20}$ m^2 s^{-1}, respectively [36]. Since both values are quite similar, the difference between the concentration gradients dC_{Fe}/dx and dC_{Cr}/dx is responsible for a flux imbalance. For the diffusion couple considered, the fluxes of iron and nickel are higher, at least by a factor of 3, than the flux of chromium. This flux imbalance between Cr and Fe/Ni leads to a local enrichment of Cr at the austenite–ferrite interface. In terms of the diffusion path this local Cr-enrichment implies that the diffusion path traverses the ($\sigma + \alpha$) two-phase field of the phase diagram, the highest Cr concentration being 26 wt.% at the ferrite–austenite interface where σ-phase eventually forms (Fig. 10).

The same procedure, i.e. plotting of the diffusion path on the Ni–Fe–Cr ternary phase diagram, was followed considering the experimentally measured data of Crofer 22 APU after exposure at 800 °C for 1000 and 3000 h (Fig. 12). In the interdiffusion profiles between the Ni-mesh and Crofer 22 APU no local enrichment of Cr

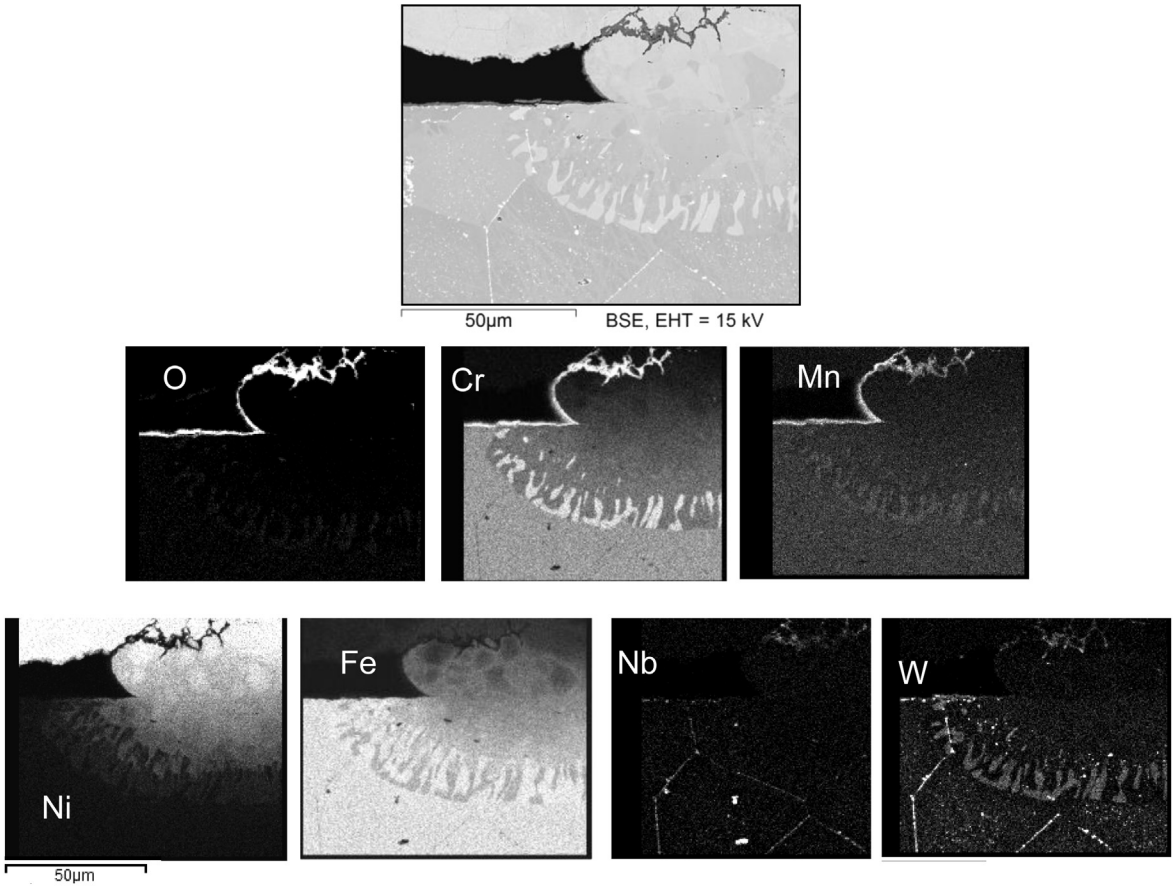

Fig. 9. BSE image of Crofer 22H in contact with a Ni-mesh after exposure in simulated anode gas, Ar–4%H_2–2%H_2O, at 700 °C for 1000 h. Lower part of the figure shows X-ray mappings of oxygen and the main alloying elements.

at the austenite–ferrite interface was observed, the reason for this being, likely, the faster diffusion of Fe, Ni and Cr at 800 °C than at 700 °C. Looking at the diffusion path it can be seen that it does not enter the $(\sigma + \alpha)$ two-phase field of the diagram and consequently no σ-phase formed. Additionally, it has to be considered that at 800 °C there is a higher chromium solubility in Fe–Ni and the $(\sigma + \alpha)$ two-phase field is therefore shifted to a higher chromium content than at 700 °C. Besides, the σ-phase stability range is smaller at 800 °C than at 700 °C.

In the case of Crofer 22H the σ-phase formation at 700 °C can be explained considering that there is a local Cr-enrichment at the ferrite–austenite interface. The measured values indicate a Cr-content in the steel substrate of 24 wt.%, of 35 wt.% Cr in the σ-phase and of 17 wt.% in the alloy matrix which results in an average Cr-content in the two-phase region of approximately 26 wt.% and therefore, in a local Cr-enrichment compared to the bulk steel. This local Cr-enrichment is responsible for σ-phase formation since it shifts the diffusion path into the $(\sigma + \alpha)$ two-phase field of the phase diagram (Fig. 10).

The σ-phase formation after 1000 h exposure at 800 °C is due to a slight Cr-enrichment at the austenite–ferrite interface and due to a higher stability of σ-phase in Crofer 22H than in Crofer 22 APU. Nonetheless, σ-phase was no longer observed after 3000 h exposure (Fig. 7). The reason for this finding is the homogenization of

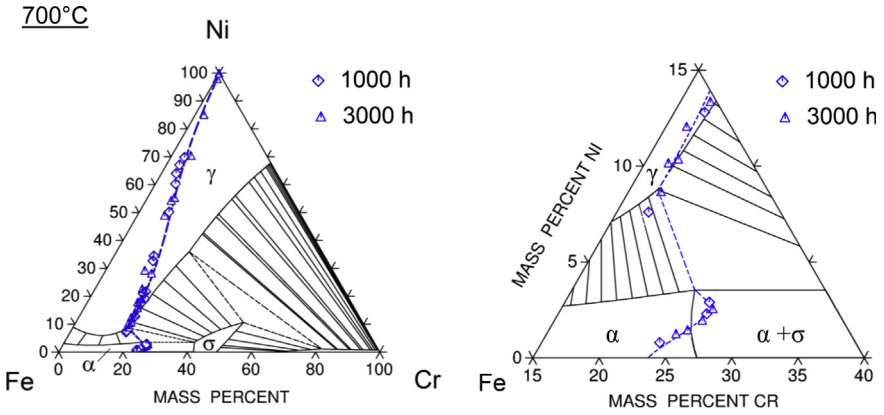

Fig. 10. Ni–Fe–Cr ternary phase diagram at 700 °C showing the experimentally measured points and diffusion path of Crofer 22 APU in contact with Ni-mesh after exposure in simulated anode gas, Ar–4%H_2–2%H_2O, at 700 °C for 1000 and 3000 h. Diagram calculated using ThermoCalc (database TCFE6). Data points taken from Fig. 1.

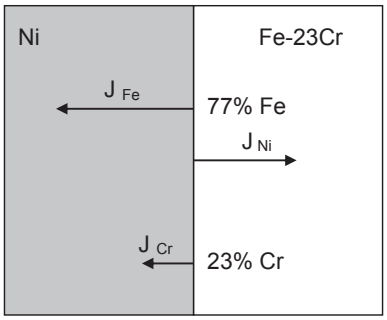

Fig. 11. Schematic of nickel/ferritic steel diffusion couple showing fluxes of iron, chromium and nickel and initial concentrations of elements (omitting minor alloying elements in ferritic steel).

the diffusion couple. In the measured interdiffusion profiles it was observed that the interface between the austenitic zone and the steel hardly moves between 1000 and 3000 h which indicated that there is a smaller Ni-reservoir as the Ni-mesh has become saturated with iron. Therefore, hardly any driving force for occurrence of a local Cr-enrichment exists and thus no σ-phase formation occurs.

More σ-phase forms at the austenite–ferrite interface in case of Crofer 22H than for Crofer 22 APU because of the different chemical compositions of the steels. Crofer 22H contains approximately 2 wt.% tungsten. Tungsten is known to stabilize σ-phase in ferritic steels [12]. The minimum amount of Cr needed for σ-phase formation has been calculated with ThermoCalc [37] using thermodynamic data from the database TCFE6 [38] considering a Fe–23Cr steel with different amounts of tungsten (Table 2). It can be seen that the amount of chromium needed for σ-phase formation decreases with increasing tungsten content. Since Crofer 22H also contains 0.5 wt.% niobium, the influence of niobium on the minimum chromium content needed for σ-phase formation was also calculated. The calculations show that niobium does not seem to play a major role in σ-phase formation. Additionally, it is worth mentioning that the amount of chromium needed for σ-phase formation is, in all cases, higher at 800 °C than at 700 °C.

According to these calculations and to the experimental results, the exact chemical composition, and more specifically the exact Cr-content, of the steel are, especially at 700 °C, governing σ-phase formation. In the data sheet for e.g. Crofer 22H the Cr-content is specified to be between 20 and 24 wt. % and the W-content between 1 and 3 wt.% [39]. This wide composition range implies that for the same material, depending on the actual steel batch used, σ-phase might form at the ferrite–austenite interface in one batch but not in another.

Considering a simplified diffusion couple of a Ni-mesh and a Fe–Cr steel and the ternary Ni–Fe–Cr phase diagram at 700 °C, three cases can be considered (Fig. 13).

1) Steel with low Cr-content (~20 wt.%): The Fe–Cr steel is initially in the α-ferrite field of the ternary phase diagram (Fig. 13). Once interdiffusion between the steel and the Ni-mesh takes place, a flux of Fe and Cr would be established towards the Ni-mesh and a flux of Ni in the opposite direction. As explained before, this would lead to a local chromium enrichment at the ferrite–austenite interface but due to the low Cr-content of the steel this Cr-enrichment would not be sufficient for the diffusion path to enter the $(\alpha + \sigma)$ two-phase field of the diagram and thus no σ-phase will form.
2) Steel with an intermediate Cr-content, (approximately 22 wt. %) as e.g. the case for the studied Crofer 22 APU and Crofer 22H. The Fe–Cr steel is, as in the previous case, initially located in the α-ferrite field of the Ni–Fe–Cr phase diagram. Nonetheless, in this case the local Cr-enrichment at the ferrite–austenite interface caused by interdiffusion processes would be sufficient to shift the equilibrium to the $(\alpha + \sigma)$ two-phase field and σ-phase would form in equilibrium with the α phase. From the $(\alpha + \sigma)$ two-phase field it is thermodynamically not possible for the system to enter the three-phase field and the diffusion path follows into the austenite stability field (γ) of the diagram, along the respective tie-line in the diagram.
3) The chemical composition of the steel with a high Cr-content (e.g. 26 wt.%) is such that the steel is already in the $(\alpha + \sigma)$ two-phase field in the initial condition. Due to interdiffusion processes between the Ni-mesh and the steel, the equilibrium would, because of the local Cr-enrichment, be shifted into the σ-phase field and a virtually continuous layer of σ-phase would form. Further diffusion of Fe, Cr, and Ni causes the system to enter the $(\gamma + \sigma)$ two-phase field, implying that σ-phase would form in equilibrium with austenite. An example of such a diffusion couple, in which a ferritic steel with 26 wt.% Cr was used as interconnect material, was experimentally observed in Ref. [40].

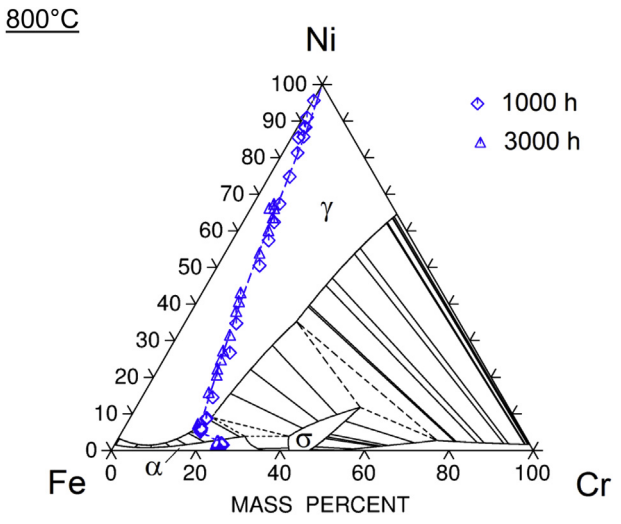

Fig. 12. Ni–Fe–Cr ternary phase diagram at 800 °C showing the experimentally measured points and diffusion path of Crofer 22 APU in contact with Ni-mesh after exposure in simulated anode gas, Ar–4%H_2–2%H_2O, at 800 °C for 1000 and 3000 h. Diagram calculated using ThermoCalc (database TCFE6). Data points taken from Fig. 1.

Figs. 7–9 show that the Fe_2(W,Nb) Laves-phase was hardly present in the austenitic zone which formed when Crofer 22H in contact with Ni-mesh was exposed at 700 and 800 °C in simulated anode gas. EDX analyses showed that the oxides formed on the Ni-mesh contain not only Cr and Mn but also small amounts of Nb. The diffusion of Nb from the steel into the Ni-mesh might be the reason for the vanishing of Laves-phase in the contact zone between the Ni-mesh and Crofer 22H. Additionally, the σ-phase formed at the

Table 2
Minimum amount of Cr (mass.-%) needed for σ-phase formation in a Fe–23%Cr steel with different amounts of W and Nb (calculations carried out using ThermoCalc (database TCFE6)).

	Fe –23Cr	Fe–23Cr –1W	Fe–23Cr –2W	Fe–23Cr –0.5Nb	Fe–23Cr–2W –0.5Nb
700 °C	25.6	24.2	23.7	25.4	23.6
800 °C	34.3	32.1	30.1	33.7	30.2

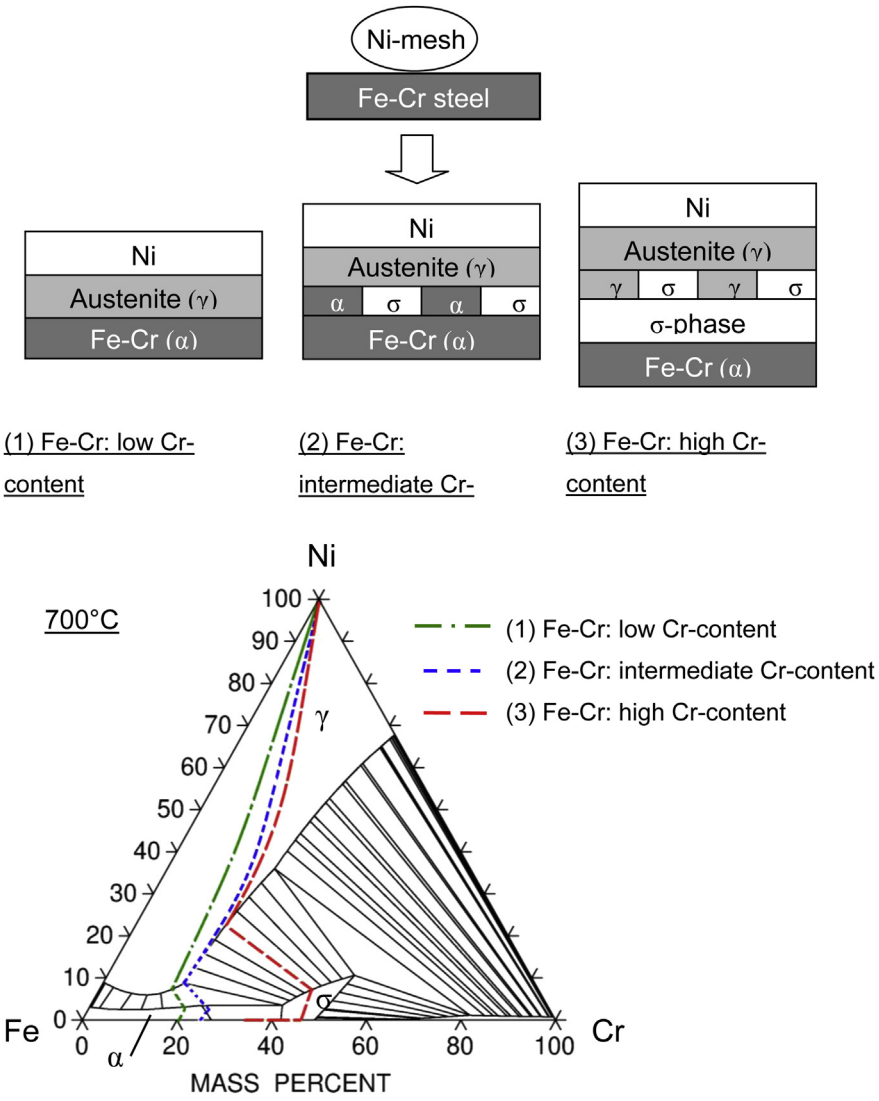

Fig. 13. Schematic representation of phase transformations in a diffusion couple between a Ni-mesh and different types of Fe–Cr steel at 700 °C. Lower part of the figure shows schematically diffusion paths in ternary phase diagram Fe–Cr–Ni of: (1) steel with low Cr-content, (2) steel with intermediate Cr-content and (3) steel with high Cr-content.

ferrite–austenite interface contains, according to EDX measurements, 5.5 wt.% W. This enrichment of tungsten in the σ-phase compared with the bulk material might also contribute to the dissolution of Laves-phase in the austenitic zone. Dissolution of Laves-phase in the austenite layer has been previously observed when Crofer 22H coated with a nickel layer was exposed at 700 °C in Ar–4%H_2–10%H_2O for 500 h [41]. The reason for Laves-phase dissolution is thought to be the enrichment of Nb in the outer part of the Ni layer and a depletion of Nb in the subsurface zone of the steel.

In spite of the fact that no contact resistance measurements were carried out, it seems that the microstructure changes at and near the steel-nickel interface do not substantially affect the electrical properties of the joint [18]. Long-term measurements with similar steel-nickel joints at 700 and 800 °C in Ar–H_2–H_2O revealed changes of the area specific contact resistance in the range of 1–3.5 mΩ cm^2 during exposure times up to 3000 h. This result indicates that possible adverse effects of the nickel–steel interaction on the electrical properties seem to be less important than changes of the mechanical and/or physical properties of the interconnect and/or nickel wire mesh.

5. Conclusions

Exposure of the commercially available ferritic steels Crofer 22 APU and Crofer 22H in contact with a nickel mesh at 700–800 °C in Ar–4%H_2–2%H_2O led to interdiffusion of alloy elements between the Ni-mesh and the steels. Ni diffuses from the Ni-mesh into the steel whereas Fe, Cr and Mn diffuse from the steel into the Ni-mesh. Diffusion of Ni into the ferritic steel led to the formation of austenite in the contact zone between the Ni-mesh and the steel whereas diffusion of Cr and Mn into the Ni-mesh led to the formation of oxides within and on the surface of the Ni-mesh.

Additionally, a number of phase transformations directly related with the interdiffusion processes have been observed. Precipitation of σ-phase occurs at the interface of the ferrite–austenite zone in Crofer 22 APU and Crofer 22H in contact with Ni-mesh after exposure at 700 °C and in Crofer 22H after exposure at 800 °C for 1000 h. The σ-phase formation is caused by a local Cr-enrichment at the austenite–ferrite interface due to a flux imbalance between Cr and Fe/Ni. Higher amounts of σ-phase form at 700 °C than at 800 °C. The σ-phase formation is more pronounced in case of Crofer 22H than for Crofer 22 APU, the reason being the σ-phase stabilising

effect of tungsten addition of 2 wt.% in Crofer 22H. The amount of σ-phase tended to decrease after longer times due to the decreasing activity gradients with prolonged exposure. In the case of Crofer 22H in contact with the Ni-mesh only minor amounts of Laves-phase precipitates were observed in the austenitic zone.

Acknowledgements

The authors are grateful to Mr. H. Cosler, Ms. A. Kick, and R. Mahnke for carrying out the oxidation tests, Mr. V. Gutzeit and Mr. J. Bartsch for optical microscopy and to Dr. E. Wessel and Dr. D. Grüner for SEM investigations. The Central Chemistry Department (ZEA) is acknowledged for the ICP-OES and IR analyses. The authors gratefully acknowledge funding from the EU project "SOFC-Life" (EU FP7/2007-2013, Fuel Cell and Hydrogen Joint Undertaking FCH-JU, project No. 256'885).

References

[1] Z. Zeng, K. Natesan, Solid State Ionics 167 (2004) 9.
[2] Z.G. Yang, K.S. Weil, D.M. Paxton, J.W. Stevenson, J. Electrochem. Soc. 150 (2003) A1188.
[3] W.J. Quadakkers, H. Greiner, W. Köck, in: Proceedings of the 1st First European Solid Oxide Fuel Cell Forum, 1994, p. 525.
[4] W.J. Quadakkers, J. Piron-Abellan, V. Shemet, L. Singheiser, Mater. High Temp. 20 (2003) 115.
[5] W.J. Quadakkers, T. Malkow, J. Piron-Abellan, U. Flesch, V. Shemet, L. Singheiser, in: Proceedings of the 4th European Solid Oxide Fuel Cell Forum 2, 2000, pp. 827–836.
[6] P. Huczkowski, N. Christiansen, V. Shemet, L. Niewolak, J. Piron-Abellan, L. Singheiser, W.J. Quadakkers, Fuel Cells 6 (2006) 93–99.
[7] K.A. Nielsen, S. Linderoth, B. Kindl, J.B. Bilde-Sørensen, P.H. Larsen, in: Presented at Fifth European Solid Oxide Fuel Cell Forum, Oberrohrdorf, Switzerland, 2002.
[8] W.Z. Zhu, S.C. Deevi, Mater. Sci. Eng. A 362 (2003) 228.
[9] P. Huczkowski, N. Christiansen, V. Shemet, J. Piron-Abellan, L. Singheiser, W.J. Quadakkers, J. Fuel Cell. Sci. Technol. 1 (2004) 30–34.
[10] P. Huczkowski, V. Shemet, J. Piron-Abellan, L. Singheiser, W.J. Quadakkers, N. Christiansen, Mater. Corros. 55 (2004) 825–830.
[11] J. Froitzheim, L. Niewolak, M. Brandner, L. Singheiser, W.J. Quadakkers, J. Fuel Cell. Sci. Technol. 7 (2010).
[12] L. Niewolak, E. Wessel, T. Huettel, C. Asensio-Jimenez, L. Singheiser, W.J. Quadakkers, J. Electrochem. Soc. 159 (2012) F725.
[13] W.A. Meulenberg, A. Gil, E. Wessel, H.P. Buchkremer, D. Stover, Oxid. Met. 57 (2002) 1.
[14] K.A. Nielsen, A.R. Dinesen, L. Korcakova, L. Mikkelsen, P.V. Hendriksen, F.W. Poulsen, Fuel Cells 6 (2006) 100.
[15] W.J. Shong, C.K. Liu, P. Yang, Mater. Chem. Phys. 134 (2012) 670.
[16] A.N. Hansson, M.B. Mogensen, S. Linderoth, M.A.J. Somers, J. Corros. Sci. Eng. 6 (2003) 12.
[17] J. Froitzheim, RWTH Aachen, Aachen, FRG (Ph.D thesis), 2008.
[18] V. Sarda, S. Auvinen, V. Shemet, W.J. Quadakkers, M. Pihlatie, J. Kiviaho, L.G.J. de Haart, ECS Trans. 57 (2013) 2279.
[19] S. Leistikow, I. Wolf, H.J. Grabke, Werkst. Korros. 38 (1987) 556.
[20] M. Thiele, H. Teichmann, W. Schwarz, W.J. Quadakkers, H. Nickel, Kraftwerkstechnik 2 (1997) 143.
[21] D.J. Young, J. Zurek, L. Singheiser, W.J. Quadakkers, Corros. Sci. 53 (2011) 2131.
[22] L. Singheiser, P. Huczkowski, T. Markus, W.J. Quadakkers, in: J.A. Richardson (Ed.), Sheir's Corrosion, vol. 1, Elsevier, Oxford, 2010, p. 482.
[23] M. Kajihara, M. Kikuchi, Acta Metall. Mater. 43 (1995) 807.
[24] R.A. Perkins, R.A. Padgett, N.K. Tunali, Metall. Trans. 4 (1973) 2535.
[25] Z. Tokei, H. Viefhaus, H.J. Grabke, Appl. Surf. Sci. 165 (2000) 23.
[26] S.C. Singhal, K. Kendall, High Temperature Solid Oxide Fuel Cells: Fundamentals, Design and Applications, Elsevier, Oxford, UK, 2006.
[27] R. Hojda, W. Heimann, W.J. Quadakkers, in: ThyssenKrupp Techforum, 2003, pp. 20–23.
[28] W.J. Quadakkers, L. Paul, H. Hattendorf, Crofer 22H - a New High Strength Ferritic Steel for Interconnectors in SOFC, Presented at Fuel Cell Symposium, San Antonio, USA, 2010.
[29] C. Asensio-Jimenez, L. Niewolak, H. Hattendorf, B. Kuhn, P. Huczkowski, L. Singheiser, W. Quadakkers, Oxid. Met. 79 (2013) 15.
[30] W.J. Quadakkers, J. Zurek, in: J.A. Richardson (Ed.), Sheir's Corrosion, vol. 1, Elsevier, Amsterdam, 2010, p. 407.
[31] J.M. Joubert, Prog. Mater. Sci. 53 (2008) 528.
[32] J. Zurek, D.J. Young, E. Essuman, M. Hänsel, H.J. Penkalla, L. Niewolak, W.J. Quadakkers, Mater. Sci. Eng. A 477 (2008) 259.
[33] B. Kuhn, C.A. Jimenez, L. Niewolak, T. Hüttel, T. Beck, H. Hattendorf, L. Singheiser, W.J. Quadakkers, Mater. Sci. Eng. A 528 (2011) 5888.
[34] C. Asensio, A. Chyrkin, L. Niewolak, V. Konoval, H. Hattendorf, B. Kuhn, L. Singheiser, W.J. Quadakkers, Electrochem. Solid State Lett. 14 (2011) P17.
[35] L. Niewolak, D.J. Young, H. Hattendorf, L. Singheiser, W.J. Quadakkers, Oxid. Met. 82 (2014) 123–143.
[36] MOB2, TCS Alloys Mobility Database, v.2.0, Royal Institute of Technology, Foundation of Computational Thermodynamics, Stockholm, Sweden, 1999.
[37] B. Jansson, M. Schalin, M. Selleby, B. Sundman, Computer Software in Chemical and Extractive Metallurgy, Canadian Inst Mining, Metallurgy and Petroleum, Montreal, 1993, p. 57.
[38] BT TTFE6, TCS Steels/Fe-alloys Database v.6.2, Royal Institute of Technology, Foundation of Computational Thermodynamics, Stockholm, Sweden, 2009.
[39] Crofer® 22H, Material Data Sheet No. 4050, ThyssenKrupp VDM, June 2010.
[40] V. Shemet, C. Geipel, Q. Fang, W.J. Quadakkers, in: EUROCORR 2013, Estoril, Portugal, 2013.
[41] G.H. Meier, L. Niewolak, R.N. Patel, in: International Collaborative Workshop on the Degradation of Materials in Extreme Environments, University of Pittsburgh, July 2013, pp. 18–19.